

Resonant Frequency Tuning System for Repeater Resonator of Resonant Inductive Coupling Wireless Power Transfer

Akihiro Konishi, Keita Fujiki, Kazuhiro Umetani, Eiji Hiraki
Graduate School of Natural Science and Technology
Okayama University
Okayama, Japan

Published in: 2019 21st European Conference on Power Electronics and Applications (EPE '19 ECCE Europe)

© 2019 IEEE. Personal use of this material is permitted. Permission from IEEE must be obtained for all other uses, in any current or future media, including reprinting/republishing this material for advertising or promotional purposes, creating new collective works, for resale or redistribution to servers or lists, or reuse of any copyrighted component of this work in other works.

DOI: 10.23919/EPE.2019.8914736

Resonant Frequency Tuning System for Repeater Resonator of Resonant Inductive Coupling Wireless Power Transfer

Akihiro Konishi, Keita Fujiki, Kazuhiro Umetani, Eiji Hiraki
OKAYAMA UNIVERSITY
3-1-1 Tsushima-naka, Kita-ku
Okayama, Japan
Tel.: +81 / (86) – 251.8115.
Fax: +81 / (86) – 251.8258.
E-Mail: p3448o58@s.okayama-u.ac.jp
URL: <http://www.ec.okayama-u.ac.jp/~epc/en/index.html>

Keywords

«Wireless power transmission», «Contactless Energy Transfer», «Circuits»

Abstract

The resonant inductive coupling wireless power transfer (RIC-WPT) is a promising technique of the wireless power transfer with comparatively large power and high efficiency. However, the performance of RIC-WPT system is generally highly dependent on the fine adjustment of the resonant frequency between the transmitter, receiver, and repeater resonators, although the natural tolerance of the capacitor and inductance of the coil may easily lead to the significant detuning of the resonant frequency. Particularly, the repeater resonator is the key item that can improve the power transfer to a distantly located receiver resonator. However, the repeater resonator tends to have a high quality-factor; and therefore, its performance can be easily deteriorated by the detuning of the resonant frequency. The purpose of this paper is to propose a simple automatic resonant frequency tuning system for the repeater resonator as a remedy for the performance deterioration due to the resonant frequency detuning. The operation of the automatic resonant frequency tuning system was experimentally tested using the prototype wireless power transfer system. The result exhibited robust power transfer capability regardless of the natural tolerance of the resonant frequency.

Introduction

Wireless power transfer (WPT) is a safe convenient power supply technology without using the wire connection. Various applications of WPT systems have been proposed in the literature, such as EVs chargers [1], [2], biomedical implants [3], and wearable devices [4], [5]. Among the various methods for WPT, the resonant inductive coupling WPT (RIC-WPT) is attracting researchers' attention because of its comparatively large output power and high efficiency. The basic RIC-WPT system comprises the transmitter resonator with the inverter, which supplies AC power to excite the resonance in this resonator, and the receiver resonator with the rectifier, which generates the DC output power, as shown in Fig. 1. These resonators are designed to have the same resonance frequency so that the weak AC magnetic field generated by the transmitter coil can induce the sufficiently large resonance in the receiver resonator. However, the RIC-WPT system can also be utilized with the repeater resonator, which can improve the power transfer capability to the distantly located receiver resonator [6]–[11].

The repeater resonator is configured as the LC resonator made of the coil and a capacitor, as shown in Fig. 1. This resonator should be also designed to have the same resonance frequency as the transmitter and receiver resonators. The repeater resonator generally has a high quality factor because this resonator contains no power load. Therefore, in the RIC-WPT system with the repeater resonator, the large resonance can be excited in the repeater resonator by the weak AC magnetic field generated by the transmitter resonator, even if the repeater resonator is placed distantly from the transmitter resonator.

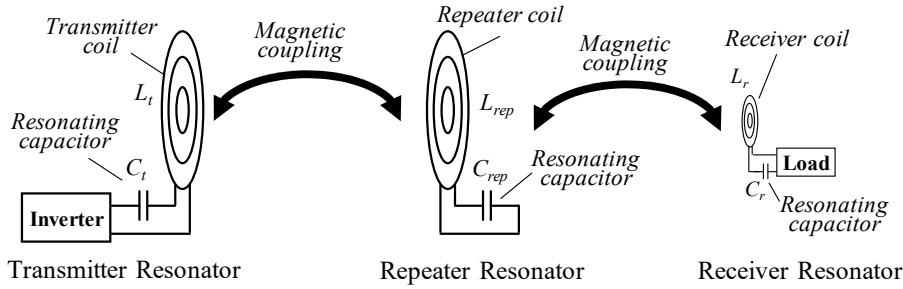


Fig. 1: Basic resonant inductive coupling wireless power transfer system with a repeater resonator.

The large resonance current of the repeater resonator generates the intense AC magnetic field near the repeater coil, which can also transfer the AC power to the receiver resonator. Consequently, the repeater resonator can expand the capable area of the wireless power transfer.

In spite of the attractive contribution of the repeater resonator, however, the main drawback is that the performance of the repeater resonator can be severely deteriorated by the detuning of the resonance frequency from that of the transmitter and receiver resonators. Because the repeater resonator has a large quality factor, only a small deviation of the resonance frequency can significantly reduce the repeater current induction. Particularly, the resonance frequency has natural tolerance due to the manufacturing tolerance and the aging deterioration of the capacitor and the inductance of the repeater coil. Furthermore, the resonance frequency is also affected by the magnetic coupling between the transmitter and receiver resonators because the high Q factor of the repeater resonator can easily cause the frequency splitting phenomenon [1], [5], [9]–[13]. Therefore, the automatic tuning system of the resonance frequency of the repeater resonator will be needed for practical application of the wireless power transfer from the viewpoint of the mass production.

There have been proposed preceding techniques in literature that can directly or equivalently vary the resonant frequency of the resonators. For example, [13] has proposed a method to vary the resonant frequency by using a variable capacitor for the resonator and mechanically adjusting the capacitance using a stepping motor. However, this method suffers from large power consumption for driving the stepping motor; and therefore, this method will greatly deteriorate the quality factor of the resonator, if applied to the repeater resonator. In order to avoid the mechanical adjustment using the stepping motor, [9], [10], and [14]–[16] have proposed electrical methods for adjusting the resonant frequency. These methods add switching circuits to generate the reactive voltage, which is added to or subtracted from the capacitor voltage to emulate the reactive voltage drop of the variable capacitance. Among these switching circuit utilized in these preceding methods, the Automatic Tuning Assist Circuit (ATAC) [9], [10], [16], [17] requires remarkably simple control, which enables to be applied to high-frequency applications.

Based on the ATAC, this paper constructs the practical automatic tuning system of the resonance frequency for the repeater resonator. The basic configuration of this system was first proposed in the recent study [9]. This preceding study elucidated the theoretical feasibility of the automatic tuning system using the ATAC, although this study did not present an actual circuit that works as the self-driven automatic tuning system. In fact, in the experiment presented in [9], the ATAC attached to the repeater resonator was connected to the transmitter resonator via wire connection to receive the DC power supply and the control signals. This problem is addressed in this paper by designing the automatic tuning system to be a fully independent system without any wire connection outside the repeater resonator and to be supplied with the power from the repeater coil current.

Proposed Automatic Resonant Frequency Tuning System

Circuit Configuration

The basic configuration of the proposed automatic frequency tuning system is shown in Fig. 2. The receiver resonator is omitted in this figure because the receiver coil, as well as its AC current, is generally

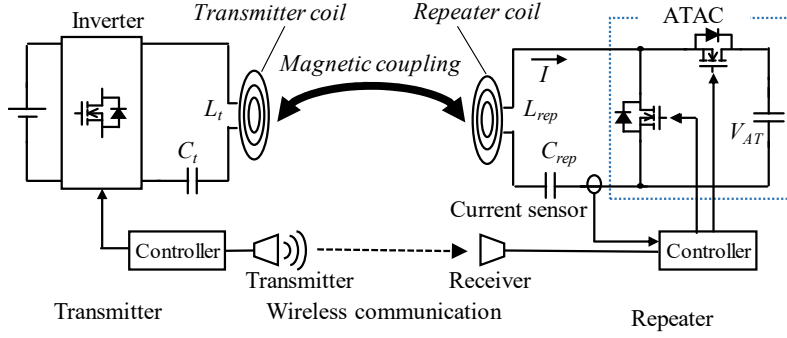


Fig. 2: Basic structure of proposed WPT system with repeater resonator and ATAC.

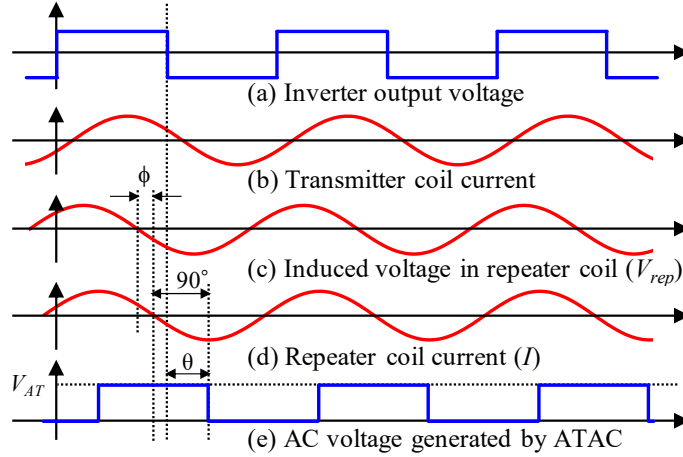


Fig. 3: Diagrams of circuit waveforms of proposed automatic tuning system.

far smaller than the repeater; and therefore, it hardly affects the overall operation of the repeater [18]. In this system, we assume that the inductance of the repeater coil L_{rep} as well as the resonating capacitor C_{rep} has a natural tolerance, which may reach $\pm 10\%$ or more. In addition to L_{rep} and C_{rep} , the ATAC is attached to the repeater resonator. The ATAC consists of a half-bridge circuit with the decoupling capacitor connected to the DC bus. The operation of the ATAC does not need any power supply except for the controller and the gate driver for the switches. The DC power for the controller and the gate driver is supplied from the DC voltage charged at the decoupling capacitor of the ATAC.

The half-bridge circuit of the ATAC should operate at the same switching frequency as the inverter of the transmitter resonator at the duty cycle of 50% but should have the optimum phase shift angle θ_{opt} to the inverter. For this purpose, the switching gate signal of one switch of the inverter is transmitted to the controller of the ATAC using the wireless communication such as the infrared communication or the electromagnetic wave communication. Based on this information, the controller of the ATAC generates the gate signals by delaying the signal received from the inverter controller via the wireless communication. The optimal phase shift angle is calculated by the controller of the ATAC so that the repeater coil current is maximized.

Controller of ATAC

Figure 3 shows the typical circuit waveforms of the proposed automatic tuning system. Because the ATAC is made as a switching circuit without any power load, the ATAC cannot receive any effective power under the steady operation. Therefore, the repeater coil current must flow at the 90-degree phase shift to the AC voltage generated by the ATAC (the mid-point voltage of the half-bridge circuit). This indicates that the controller of the ATAC can adjust the phase angle of the repeater coil current to have any desired phase shift to the signal received from the inverter controller.

Note that the induced voltage of the repeater coil must also have the same frequency as the inverter of the transmitter resonator and has the constant phase shift to the inverter because the induced voltage

must have the 90-degree phase shift to the transmitter current. Therefore, the fact that the ATAC can adjust the phase of the repeater coil current at any desired phase angle to the inverter readily indicates that the ATAC can adjust the phase difference ϕ between the induced voltage in the repeater coil and the repeater coil current. Noticing that the ATAC itself works as a pure reactance, the effective value of the repeater coil current I_{rep} can be expressed as

$$R_{rep} I_{rep}^2 = V_{rep} I_{rep} \cos \phi. \quad \therefore I_{rep} = \frac{V_{rep}}{R_{rep}} \cos \phi. \quad (1)$$

where R_{rep} is the AC resistance of the repeater coil, and V_{rep} is the effective value of the induced voltage.

This equation indicates that the maximum repeater coil current can be achieved by setting ϕ at the 0 degree. (As can be seen in (1), ϕ cannot take a value between 90–270 degree.) However, this phase difference ϕ is unknown from the controller of the ATAC because the only sensor implemented in the controller of the ATAC is the current sensor, which outputs the DC voltage proportional to the AC current amplitude of the repeater coil current. Consequently, the controller can assume that there is the unique optimum value of ϕ and therefore the unique optimum value θ_{opt} in the phase shift angle θ between the switching signal of the inverter and the ATAC switching signal, although the exact value of θ_{opt} is unknown. Therefore, the controller of the ATAC determines θ_{opt} by the hill climbing algorithm.

As we have seen, the control principle does not depend on the reactance of the repeater coil nor the resonating capacitor. Therefore, the repeater coil current of the proposed system can be maximized regardless of the resonant frequency of L_{rep} and C_{rep} . However, from the practical point of view, the sum of the reactance of L_{rep} and C_{rep} should take a small positive value so that the half-bridge circuit of the ATAC should operate under the zero-voltage switching condition, which is effective for reducing the switching loss. Therefore, in this system, we assume that the resonant frequency of the repeater was set at slightly lower than the resonant frequency of the transmitter resonator so that the ATAC can always operate at the zero voltage switching condition, even if there is a tolerance of the resonant frequency.

Design of Automatic Resonant Frequency Tuning System

Overview

A simple prototype of the proposed automatic resonant frequency tuning system was designed and constructed for evaluating the practical effectiveness. This section presents the detailed circuit design of the proposed system and the design considerations.

Figure 4 shows the block diagram of the practical circuit configuration of the proposed system including the control circuit. (For simplifying the discussion, the receiver resonator is also omitted in this figure.) The left half of the main circuit is the transmitter resonator with the inverter, whereas the right half is the repeater resonator including the ATAC. In this circuit, the resonating capacitor of the repeater resonator is implemented as a series connection of two capacitors C_{rep1} and C_{rep2} . The circuit surrounded by the dotted blue lines is the control circuit of the ATAC.

The control circuit implements the automatic resonant frequency tuning control. The controller of the inverter transmits the switching gate signal (the duty ratio is 50%) of the inverter using the infrared LED. This signal is received by the infrared photodiode of the controller of the ATAC.

The received signal v_{pd} is provided to the saw wave generating circuit to generate the double frequency saw wave v_{saw} whose falling edge synchronizes with both of the rising and falling edge of the received signal v_{pd} . Then, the saw wave v_{saw} is compared with the DC voltage signal V_{DAC} provided by the microprocessor to generate a square wave v_{cp} with a phase-shift to the saw wave. The resultant square wave v_{cp} is then provided to the half-frequency divider, to finally obtain the square wave v_g with a phase shift to the received signal v_{pd} at the infrared photodiode. Finally, this square wave v_g is provided to the

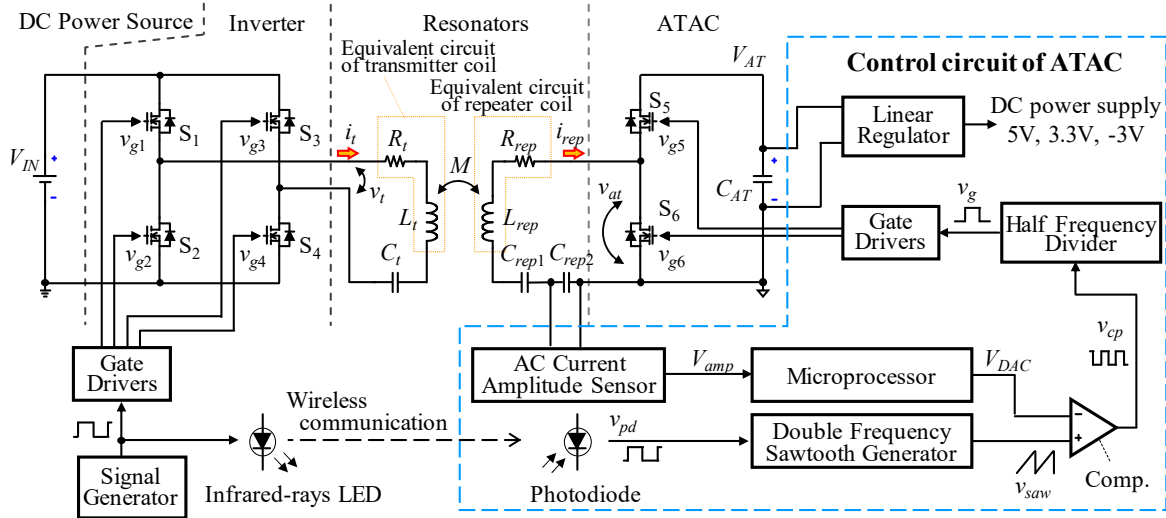


Fig. 4: Practical configuration of the RIC-WPT system with the proposed automatic resonant frequency tuning system.

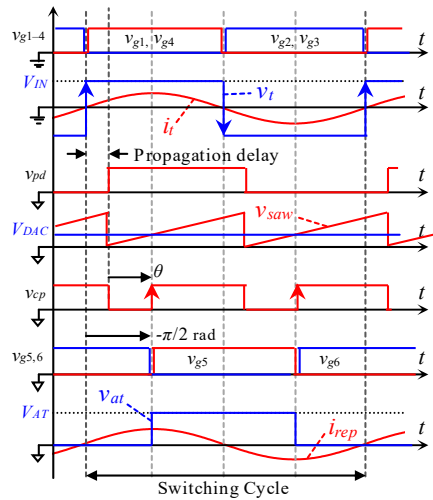


Fig. 5: Operating waveforms of proposed automatic resonance frequency tuning system.

gate drivers to drive the switches of the ATAC. The diagram of the operating waveforms is presented in Fig. 5.

As we have seen, the phase shift angle between v_{pd} and v_g is determined by the DC voltage V_{DAC} , provided by the microprocessor. This microprocessor detects the amplitude of the repeater coil current by observing the output of the AC current amplitude sensor. Then, the microprocessor searches for the optimal DC voltage that results in the maximum repeater coil current amplitude using the hill climbing algorithm.

The power of the whole control circuit as well as the gate drivers in the repeater resonator is provided from the DC voltage charged in the decoupling capacitor C_{AT} of the ATAC. The linear regulator is utilized to generate the necessary voltage for the control circuit. Because the power consumption of the control circuit appears as the additional AC resistance of the repeater resonator, the power consumption of the control circuit should be minimized to avoid deteriorating the Q factor of the repeater resonator. Particularly, the low power consumption microprocessor should be chosen for the proposed system.

Detailed Control Circuit

Figure 6 shows the schematics of the circuit blocks constituting the controller of the repeater resonator. Figure 6(a) shows the schematics of the wireless communication between the transmitter and repeater

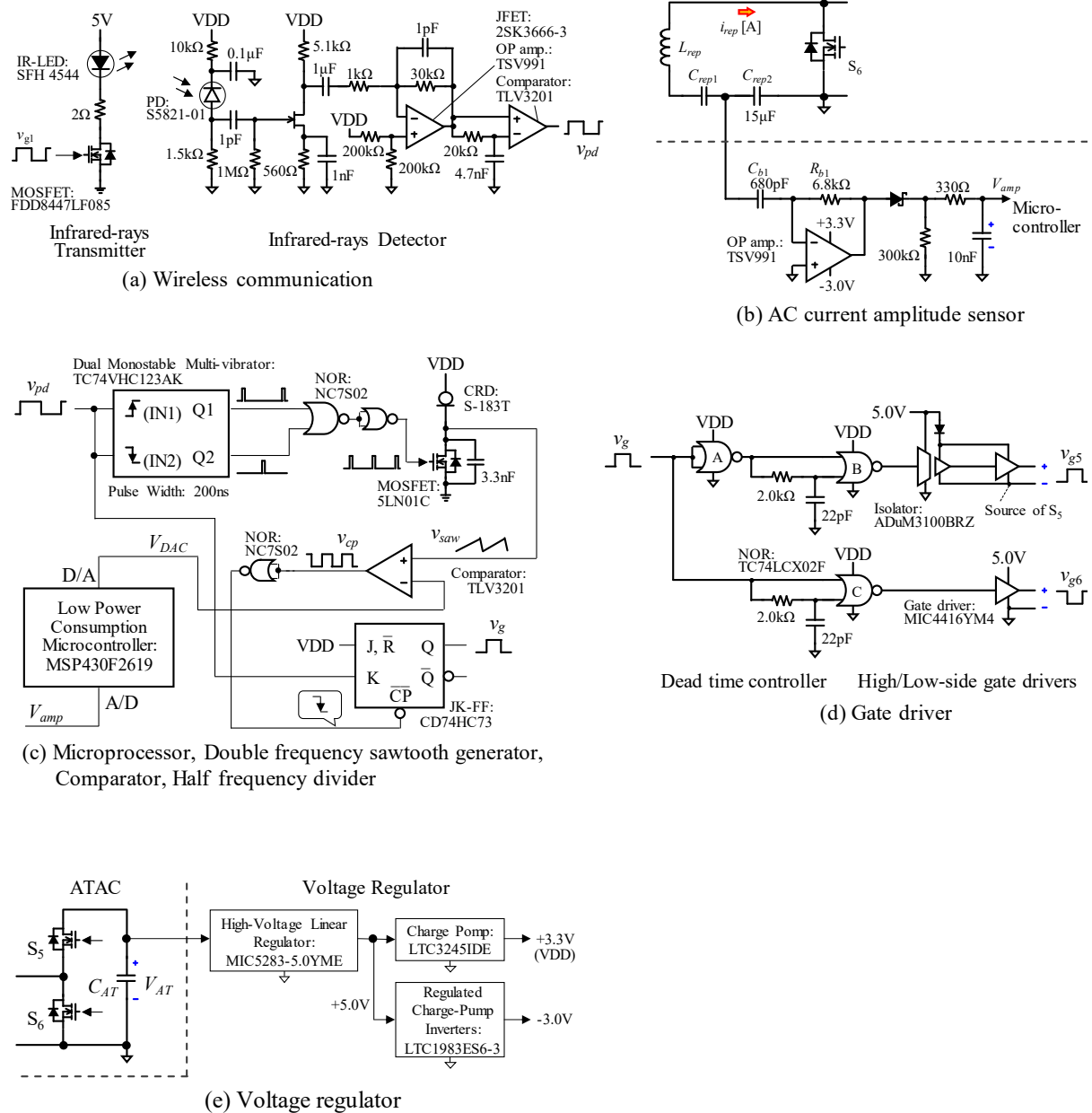


Fig. 6: Circuit diagrams of the control blocks of the control circuit of the ATAC.

resonators. In this paper, we adopted a simplest infrared-ray communication for simple construction of the prototype. The switching gate signal for S_1 is directly provided to the LED driver. Therefore, the infrared LED, which emits the infrared-ray of 950nm, is driven at the duty ratio of 50%. Then, the infrared-ray signal is received by the photodiode, which has a peak sensitivity at 960nm. Finally, the output signal of the photodiode is amplified by the JFET transistor and the op-amp and reshaped using the comparator to output the square wave signal.

Figure 6(b) shows the schematics of the AC current amplitude sensor. The amplitude sensor was comprised of the voltage differentiator and the half-wave rectifier. The voltage differentiator performed the time-differentiation of the voltage appearing at C_{rep2} . Therefore, the output of the voltage differentiator was proportional to the repeater coil current. The output of the voltage differentiator was then provided to the half-wave rectifier to detect its peak voltage, which was proportional to the amplitude of the repeater coil current. Because C_{b1} was designed to be far smaller than C_{rep2} , the relation between the resultant DC voltage output V_{amp} and the effective value of the repeater coil current I_{rep} is

$$V_{amp} = \frac{\sqrt{2}C_{b1}}{C_{rep2} + C_{b1}} R_{b1} I_{rep} \approx \frac{\sqrt{2}C_{b1}}{C_{rep2}} R_{b1} I_{rep}. \quad (2)$$

The sensing gain can be higher by increasing C_{b1} or R_{b1} and reducing C_{rep2} . However, large C_{b1} or small C_{rep2} results in increase of the power consumption at this circuit block because the AC current through C_{b1} leads to the power loss. Therefore, the prototype was designed to keep C_{b1} as small as possible (but sufficiently larger than the input capacitance of the op-amp) and C_{rep2} as large as possible to minimize the power loss at the control circuit.

Figure 6(c) shows the schematics of the control blocks that generates the gate signals. For minimizing the power consumption at the control circuit, these blocks were designed to have the simplest circuit, similarly as the other blocks of the control circuit. The double frequency sawtooth generator was designed using a dual monostable multi-vibrator, a NOR gate, and a current regulative diode (CRD). The half-frequency divider is designed using a NOR gate and a JK-Flipflop (FF). Output of the JK-FF, i.e. the gate signals for S5 and S6, is supplied to the gate driver, shown in Fig. 6(d). Low power consumption microprocessor generates the command value V_{DAC} for the phase difference according to the hill climbing algorithm. Control algorithm of the microprocessor is shown in Fig. 7.

Figure 6(e) shows the schematics of the DC power supply to the control circuit. The DC voltage V_{AT} of the decoupling capacitor of the ATAC can vary in a wide range of value. Therefore, the high-voltage linear regulator was employed to generate the medium DC voltage source of 5.0V; and then, the DC voltage source of +3.3V/-3.0V was generated using the charge-pumps to reduce the power loss by the linear regulator.

Voltage Tolerance for Switches and Decoupling Capacitor

A high voltage may appear at the decoupling capacitor C_{AT} of the ATAC. Therefore, an appropriate design of the voltage tolerance is important for C_{AT} and the switching devices S5 and S6. This subsection presents the analytical calculation of V_{AT} for design of the voltage tolerance.

Noticing that the AC voltage generated by the ATAC has the 90-degree phase shift to the repeater coil current and neglecting all the harmonics, V_{AT} can be approximated to have the following relation by applying Kirchhoff's law of voltage to the repeater resonator as

$$\frac{\sqrt{2}}{\pi} V_{AT} = ZI - V_{rep} \sin \phi. \quad (3)$$

where Z is the sum of the reactance of L_{rep} and C_{rep} . Substituting (1) into (3), we have

$$V_{AT} = \frac{\pi}{\sqrt{2}} V_{rep} \left(\frac{Z}{R_{rep}} \cos \phi - \sin \phi \right). \quad (4)$$

We can assume $Z/R_{rep} \gg 1$ in many practical design of the repeater coil (for achieving the zero voltage switching of the ATAC) and ϕ takes a value close to 0 as a result of the control. Consequently, (4) can be approximated as

$$V_{AT} \approx \frac{\pi}{\sqrt{2}} V_{rep} \frac{Z}{R_{rep}} = \frac{\pi}{\sqrt{2}} \omega M I_t \frac{Z_{rep}}{R_{rep}} \frac{Z}{Z_{rep}} = \sqrt{2} \pi \omega M Q \frac{\Delta f}{f_{res}} I_t. \quad (5)$$

where M is the mutual inductance between the transmitting and repeater coils, I_t is the effective value of the transmitter coil current, ω is the angular operating frequency, f_{res} is the resonance frequency of the repeater resonator, Z_{rep} is the reactance of the repeater coil at f_{res} , Δf is the difference of the driving frequency of the transmitter coil from f_{res} , and Q is the quality factor of the repeater resonator. The result

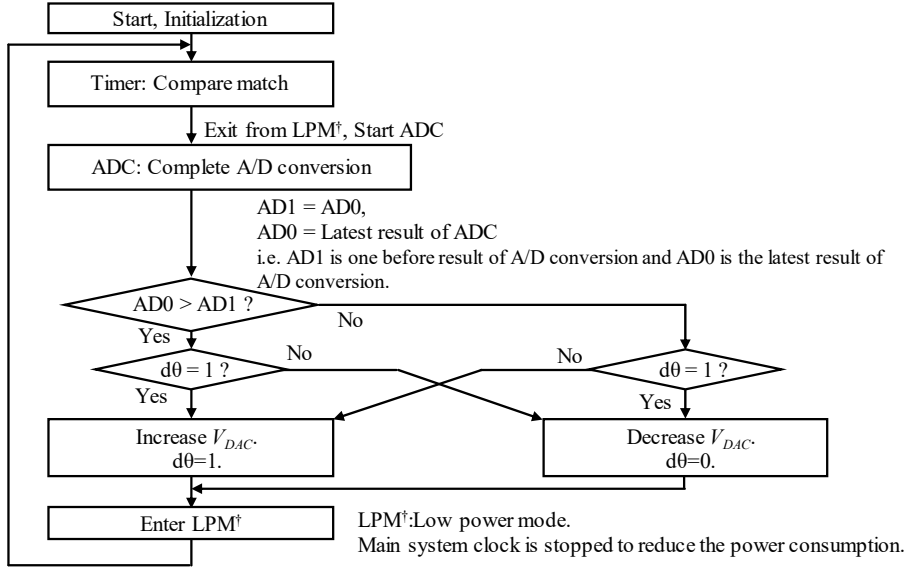


Fig. 7: The block diagram of the hill climbing algorithm performed by the microprocessor.

indicates that the large tolerance is needed, particularly if the frequency deviation Δf is large. (Certainly, (5) indicates that smaller M and Q will reduce V_{AT} . However, reducing M and Q results in smaller current induction in the repeater coil, deteriorating the performance of the repeater coil.)

Experiment

The experiment was carried out to verify the proposed automatic resonant frequency tuning system for the RIC-WPT. Table I shows the specifications of the experiment. The experimental prototype was constructed according to the specifications. This prototype does not have the receiver resonator because the purpose of this experiment is to evaluate the stable induction of the repeater coil current. Figure 8 shows the photographs of the prototype: Fig. 8(a) shows the transmitter and repeater coils; Fig. 8(b) shows the printed circuit board of the repeater resonator, which contains the control circuit of the ATAC; Fig. 8(c) shows the infrared wireless communication circuit. In this experiment, the infrared photodiode is located at the distance of 24mm from the infrared LED.

In this experiment, we compared the performance between the prototype with and without the proposed automatic resonant frequency tuning system. (Hence, the repeater resonator contains only L_{rep} and C_{rep1} in the prototype without the proposed system.) In this experiment, the repeater coil current was evaluated under various deviation of the resonant frequency of the repeater resonator from its required value. As

Table I: Specifications of experiment

Component	Symbol	Value
Input DC voltage	V_{IN}	3.5 V
Parasitic resistance in transmitter resonator	R_t	0.12 Ω
Parasitic resistance in repeater resonator	R_{rep}	0.12 Ω
Resonant inductance in transmitter coil	L_t	36.4 μH
Resonant inductance in repeater coil	L_{rep}	36.3 μH
Resonant capacitance in transmitter resonator	C_t	17.40 nF
Resonant capacitance in repeater resonator with proposed system	C_{rep1}	20.61 nF
without proposed system		17.44 nF
Voltage-dividing capacitor	C_{rep2}	15 μF
ATAC capacitance	C_{AT}	25 μF
Mutual inductance	M	5.78 μH
Coupling coefficient	k	0.16
Resonant frequency	f_r	200 kHz
Operating frequency	f_{op}	218 kHz

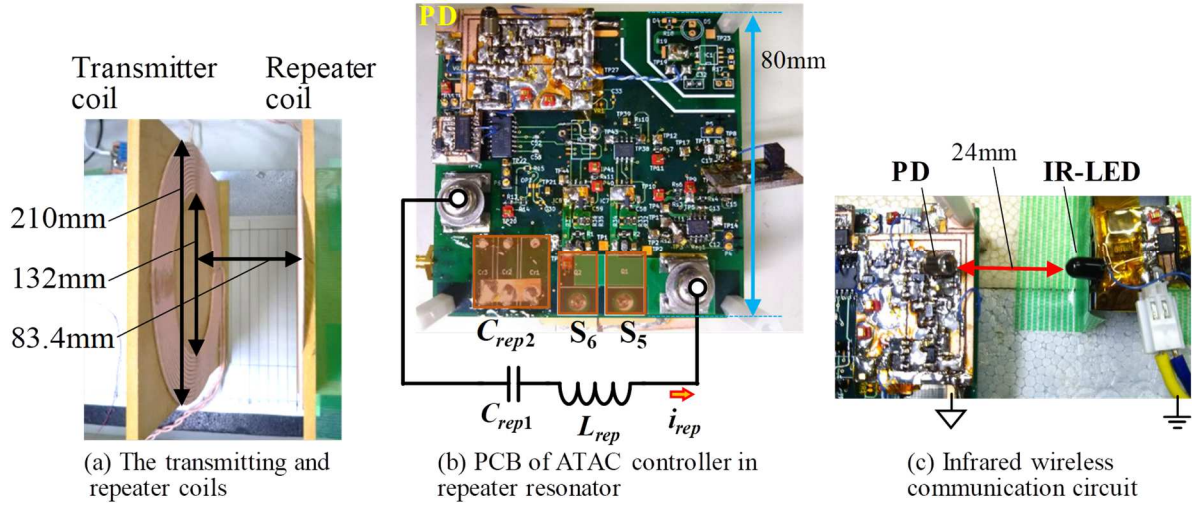


Fig. 8: The photographs of the prototype.

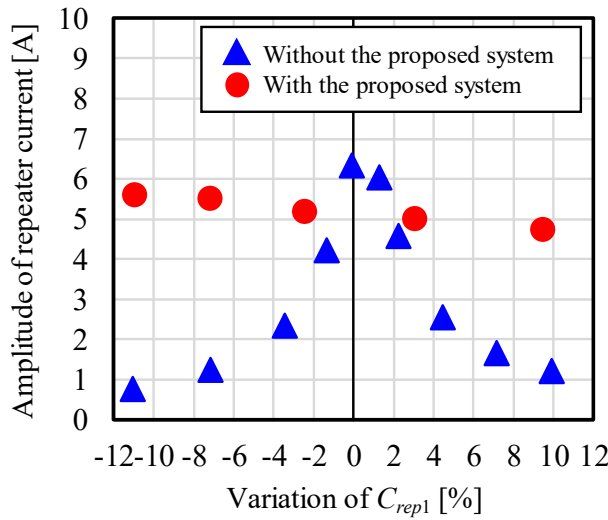


Fig. 9: The experimental result.

for the prototype without the proposed system, this required value is 200kHz, which is identical to the resonant frequency of the transmitter resonator. Meanwhile, in the prototype with the proposed system, this required value is 184kHz, which is 8% smaller than that of the transmitter resonator for the soft switching of the ATAC. We varied the capacitance of the resonating capacitor C_{rep1} for $\pm 10\%$ and evaluated the repeater coil current dependence on the deviation of the resonant frequency. Then, we compared the dependence between with and without the proposed system.

Figure 9 shows the experimental result. As can be seen in the figure, the prototype with the proposed system showed almost constant repeater coil current regardless of the variation of C_{rep1} , whereas the prototype without the proposed system suffers great deterioration of the repeater coil current due to the variation of C_{rep1} . Certainly, the repeater coil current in the prototype without the proposed system is greater than that with the proposed system, where the variation of C_{rep1} is almost 0%, because the proposed system adds the small equivalent AC resistance and slightly deteriorates the Q factor of the repeater resonator due to the power supply to the controller of the ATAC. However, the repeater coil current of the prototype with the proposed system was kept larger than that without the proposed system in a wider range of the variation of C_{rep1} . Consequently, the results supported the effectiveness of the proposed automatic resonant frequency tuning system.

Conclusion

The repeater resonator for RIC-WPT technology is effective for expanding the capable area of the wireless power transfer. However, due to the high Q factor of the repeater resonator, the performance of this resonator is unstable, strongly affected by the tolerance of the resonant frequency. This paper proposed an automatic resonant frequency tuning system for the repeater resonator, which successfully revealed stable and large repeater coil current regardless of the variation of the resonant frequency.

References

- [1]. Wang C.-S., Covic G. A., Stielau O. H.: Power transfer capability and bifurcation phenomena of loosely coupled inductive power transfer systems, *IEEE Trans. Ind. Electron.* Vol. 51, no. 1, pp. 148–157
- [2]. Moon S.C., Moon G.-W.: Wireless power transfer system with an asymmetric four-coil resonator for electric vehicle battery chargers, *IEEE Trans. Power Electron.* Vol. 31, no. 10, pp. 6844–6854
- [3]. Na K., Jang H., Ma H., Bien F.: Tracking optimal efficiency of magnetic resonance wireless power transfer system for biomedical capsule endoscopy, *IEEE Trans. Microw. Theory Techn.* Vol. 63, no. 1, pp. 295–304
- [4]. Basar M. R., Ahmad M. Y., Cho J., Ibrahim F.: An improved wearable resonant wireless power transfer system for biomedical capsule endoscope, *IEEE Trans. Ind. Electron.* Vol. 65, no. 10, pp. 7772–7781
- [5]. Schormans M., Valente V., Demosthenous A.: Practical inductive link design for biomedical wireless power transfer: a tutorial, *IEEE Trans. Biomed. Circuits Syst.* Vol. 12, no. 5, pp. 1112–1130
- [6]. Ahn D., Hong S.: A study on magnetic field repeater in wireless power transfer, *IEEE Trans. Ind. Electron.* Vol. 60, no. 1, pp. 360–371
- [7]. Koyama T., Honjo T., Umetani K., Hiraki E.: Lagrangian derivation and analysis of a simple equivalent circuit model of wireless power transfer system with dual transmitting resonators, *Proc. Eur. Conf. Power Electron. Appl. (EPE'16)*, pp. P1–P10.
- [8]. Jayathurathnage P. K. S., Alphones A., Vilathgamuwa D. M.: Optimization of a wireless power transfer system with a repeater against load variations, *IEEE Trans. Ind. Electron.* Vol. 64, no. 10, pp. 7800–7809
- [9]. Ishihara M., Ohata S., Fujiki K., Umetani K., Hiraki E.: Improving robustness against variation in resonance frequency for repeater of resonant inductive coupling wireless power transfer systems, *Proc. Eur. Conf. Power Electron. Appl. (EPE'18)*, pp. P1–P9
- [10]. Ishihara M., Umetani K., Hiraki E.: Impedance matching to maximize induced current in repeater of resonant inductive coupling wireless power transfer systems, *Proc. IEEE Energy Conversion Congr. Expo. (ECCE 2018)*, pp. 6194–6201
- [11]. Lee K., Chae S. H.: Power transfer efficiency analysis of intermediate-resonator for wireless power transfer, *IEEE Trans. Power Electron.* Vol. 33, no. 3, pp. 2484–2493
- [12]. Huang R., Zhang B., Qiu D., Zhang Y.: Frequency splitting phenomena of magnetic resonant coupling wireless power transfer, *IEEE Trans. Magn.* Vol. 50, no. 11, 8600204
- [13]. Trigui A., Hached S., Mounaim F., Ammari A. C., Sawan M.: Inductive power transfer system with self-calibrated primary resonant frequency, *IEEE Trans. Power Electron.* Vol. 30, no. 11, pp. 6078–6087
- [14]. Mai R., Liu Y., Li Y., Yue P., Cao G., He Z.: An active-rectifier-based maximum efficiency tracking method using an additional measurement coil for wireless power transfer, *IEEE Trans. Power Electron.* Vol. 33, no. 1, pp. 716–728
- [15]. Osawa J., Isobe T., Tadano H.: Efficiency improvement of high frequency inverter for wireless power transfer system using a series reactive power compensator, *Proc. IEEE Power Electron. Drive Syst. Conf. (PEDS 2017)*, pp. 992–998
- [16]. Endo Y., Furukawa Y.: Proposal for a new resonance adjustment method in magnetically coupled resonance type wireless power transmission, *Proc. Int. Microw. Workshop Series on Innovative Wireless Power Transmission: Tech., Syst., and Appl. (IMWS-IWPT)*, pp. 263–266
- [17]. Kamaeguchi K., Umetani K., Hiraki E.: Application of automatic resonant frequency tuning circuit to induction heating system, *Proc. European Conf. Power Electron. Appl. (EPE2018)* pp. 1–8.
- [18]. Mao S., Zhang J., Song K., Wei G., Zhu C.: Wireless power transfer using a field-enhancing coil and a small-sized receiver with low coupling coefficient, *IET Power Electron.* Vol. 9, no. 7, pp. 1546–1552